First-principles study of structural, electronic, vibrational, dielectric and elastic properties of tetragonal Ba2YTaO6

C. Ganeshraj and P. N. Santhosh

Citation: Journal of Applied Physics **116**, 144104 (2014); doi: 10.1063/1.4897452
View online: http://dx.doi.org/10.1063/1.4897452
View Table of Contents: http://scitation.aip.org/content/aip/journal/jap/116/14?ver=pdfcov
Published by the AIP Publishing

First-principles study of structural, electronic, vibrational, dielectric and elastic properties of tetragonal Ba_2YTaO_6

C. Ganeshraj and P. N. Santhosh[a)]
Low Temperature Physics Laboratory, Department of Physics, Indian Institute of Technology Madras, Chennai 600 036, Tamil Nadu, India

(Received 15 August 2014; accepted 27 September 2014; published online 13 October 2014)

We report first-principles study of structural, electronic, vibrational, dielectric, and elastic properties of Ba_2YTaO_6, a pinning material in high temperature superconductors (HTS), by using density functional theory. By using different exchange-correlation potentials, the accuracy of the calculated lattice constants of Ba_2YTaO_6 has been achieved with GGA-RPBE, since many important physical quantities crucially depend on change in volume. We have calculated the electronic band structure dispersion, total and partial density of states to study the band gap origin and found that Ba_2YTaO_6 is an insulator with a direct band gap of 3.50 eV. From Mulliken population and charge density studies, we conclude that Ba_2YTaO_6 have a mixed ionic-covalent character. Moreover, the vibrational properties, born effective charges, and the dielectric permittivity tensor have been calculated using linear response method. Vibrational spectrum determined through our calculations agrees well with the observed Raman spectrum, and allows assignment of symmetry labels to modes. We perform a detailed analysis of the contribution of the various infrared-active modes to the static dielectric constant to explain its anisotropy, while electronic dielectric tensor of Ba_2YTaO_6 is nearly isotropic, and found that static dielectric constant is in good agreement with experimental value. The six independent elastic constants were calculated and found that tetragonal Ba_2YTaO_6 is mechanically stable. Other elastic properties, including bulk modulus, shear modulus, Young's modulus, Poisson's ratio, and elastic anisotropy ratios are also investigated and found that Poisson's ratio and Young's modulus of Ba_2YTaO_6 are similar to that of other pinning materials in HTS. © *2014 AIP Publishing LLC*. [http://dx.doi.org/10.1063/1.4897452]

I. INTRODUCTION

For many decades, transition metal oxides have received much attention owing to their diverse properties like colossal dielectric constant,[1] magnetoresistance,[2] high temperature superconductors (HTS),[3] magnetocaloric effect,[4] and magnetoelectric effect.[5] Perovskite and its structurally related oxides have been widely studied due to their interesting physical properties and extensive structural diversity. Even though many compounds adopt the ideal cubic perovskite aristotype, most perovskites undergo a distortion away from high-symmetry cubic structure.[6] Perovskite oxide has the general stoichiometry ABO_3 and is composed of corner-sharing BO_6 octahedra with A-site cation occupying void created by the three dimensional octahedral network. Thus, the B cations are at the centers of the octahedra, while the A cations occupy 12-fold- coordinated sites. This ideal structure, which is usually described by lattice parameter a_p, displays a wide variety of structural instabilities in the various materials. The low symmetry structure can be described as a distorted structure with respect to ideal cubic structure. These distortions often influence the physical properties and remarkable structural chemistry has been observed in these materials. These distortions may involve rotations and distortions of the BO_6 octahedra as well as displacements of the cations from their ideal sites. The most common distortion consists of rigid unit modes (RUM), where BO_6 octahedra remain almost rigid and the rotation of octahedra generates antiferrodistortive distortion. The second type of distortion is ferroelectric, where the A or B cations are displaced against rigid BO_6 octahedra. The third type of distortion involves deformation of BO_6 octahedra. A detailed study on the octahedral tilting in cation ordered double perovskite using number of technique, including group theoretical analysis,[7] has been examined by various groups. The family of double perovskite $Ba(B'_{1/2}\ B''_{1/2})O_3$ have been investigated in last two decades for their microwave and infrared dielectric properties. Among double perovskites, Ba_2YTaO_6 (BYTO) undergoes an equitranslational improper ferroelastic second order phase transition from cubic ($Fm\text{-}3\,m$) to tetragonal ($I4/m$) structure without any unit cell multiplication, characterized by the tilting of the oxygen octahedra (Glazer's notation: $a^0a^0c^-$) along c-axis, around 253 K.[8] A pressure induced phase transition from cubic to tetragonal structure is also observed between 4.3 and 5.6 GPa with a onset of an octahedral tilting distortion about c-axis.[9] Recently, BYTO has been used in a form of nanocomposites with $YBa_2Cu_3O_7$, as an artificial pinning centres immobilizing quantized vortices in HTS, to enhance the ability of HTS to carry electrical current with zero resistance at high temperature and magnetic fields.[10] Also, BYTO is a useful microwave dielectric resonator material with $\varepsilon \sim 32$ near room temperature with very low dielectric loss.[8]

[a)]Email: santhosh@physics.iitm.ac.in. Tel.: +91 44 2257 4882. Fax: +91 44 2257 4852.

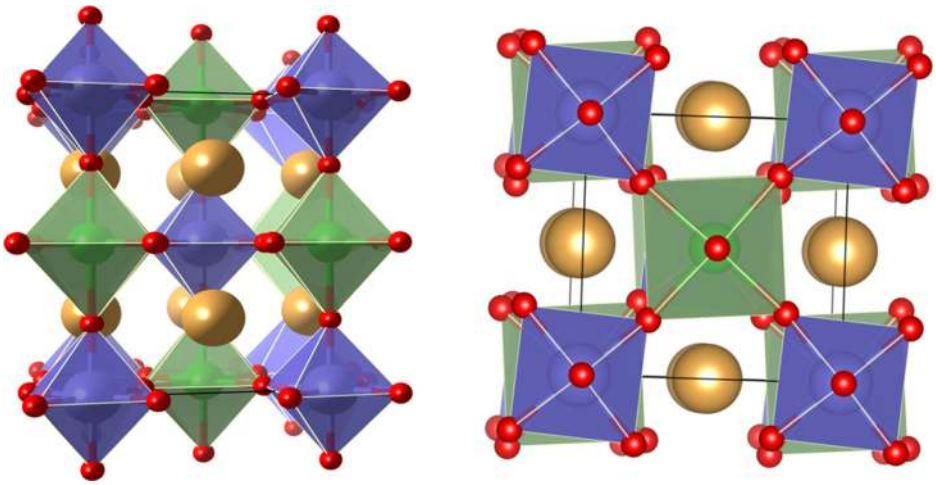

FIG. 1. Crystal structure of tetragonal (I4/m) unit cell of BYTO projected along ac and ab planes. Yellow and Red balls are represents Ba and O ions. The violet and green octahedra represent TaO_6 and YO_6. This figure was drawn using VESTA.[17]

In this paper, we present *ab initio* study of the structural, electronic, vibrational, dielectric, and elastic properties of tetragonal BYTO. We have calculated structural parameters, electronic band structure and electronic density of states (DOS), and nature of bonding of BYTO. Lattice dynamical properties, including zone-centre vibrations, Born effective charge, and electronic and static dielectric permittivity tensors, are calculated by first principles linear response method. A detailed analysis of the contribution of the various infrared-active modes to the static dielectric constant has been done to explain its anisotropy. In addition to that, we have also calculated the elastic constants, bulk modulus of BYTO using first-principles method.

II. COMPUTATIONAL DETAILS

The calculations were performed based on density functional theory (DFT) using CAmbridge Serial Total Energy Package code (CASTEP) with local-density approximation (LDA) and generalized gradient approximation (GGA).[11] The interaction of electrons with ion cores was represented by norm conserving pseudopotential for Ba ($5s^2\ 5p^6\ 6s^2$), Y ($4s^2\ 4p^6\ 4d^1\ 5s^2$), Ta ($5d^3\ 6s^2$), and O ($2s^2\ 2p^4$). A plane wave basis set with cut off energy 690 eV was used to expand the valance electronic wave functions. The exchange-correlation potential used in the calculations is LDA, GGA, GGA-PBE, GGA-PW91, and GGA-RPBE. The sampling of Brillouin zone was carefully tested and based on these convergence tests, a k-point grid of $4 \times 4 \times 3$ was used. A $12 \times 12 \times 9$ k-point grid was used for calculating vibrational properties. The Broyden-Fletcher-Goldfarb-Shanno (BFGS) minimization scheme was used in geometry optimization.[12] The geometry optimization is performed with the experimentally observed cell parameters and internal coordinates of ions,[13,14] until the maximum energy, force, stress, and displacement on the system converge to the tolerance values of 10^{-5} eV, 0.03 eV/Å, 0.05 GPa, and 0.001 Å, respectively. The lattice dynamics of BYTO is studied by density functional perturbation theory (DFPT) within the theory of linear reponse.[15] This method includes calculations of charge response to the lattice distortions for the specified vectors in the first Brillouin zone. The frequencies and displacement patterns of the phonon modes were calculated using the dynamical matrix method.

III. RESULTS AND DISCUSSION

A. Crystal and electronic structure

BYTO possesses a tetragonal structure (*I4/m*), with c-axis (tetragonal and optical axis) as a high symmetry axis, corresponding to an out of phase tilting of the octahedra around four-fold c-axis (Glazer's notation: $a^0a^0c^-$ (Ref. 16)). *I4/m* has the structural equivalence between a-axis and b-axis as well as structural difference between a-axis/b-axis and c-axis. The optimized crystal structure along ac and ab plane is illustrated in Figure 1. Table I shows the results of optimized lattice parameters obtained using the GGA-RPBE method along with LDA, GGA, GGA-PBE, GGA-PW91, and available experimental results. These results are consistent with the fact that LDA often underestimates lattice constant, while GGA reduces this error considerably.[18] The optimized internal co-ordinates of BYTO are given in Table II along with available experimental values. Figure 2 shows the calculated band structure along the high symmetry directions and the observed bandgap is ~3.50 eV between the valance band maximum and the conduction band minimum along Γ-point. Unfortunately, we have been unable to find the experimental values of the energy gap in the literature. But, it is known that the GGA calculation underestimates the band gap of semiconductors and insulators.[19] The lowest valence bands occur between −11 and −10 eV and are essentially dominated by Ba 5p states with small presence of O 2s and 2p states and non-negligible presence from O 3d to Y/Ta 3p states. The valence band lies between ~−4.5 and 0 eV (E_F), which is derived mainly from O 2p states but also, there is a quite strong hybridization between

TABLE I. Calculated (LDA, GGA-RPBE, GGA-PBE, and GGA-PW91) and experimental lattice constant and volume of Ba_2YTaO_6.

	LDA	GGA-RPBE	GGA-PBE	GGA-PW91	Exp.
a, b (Å)	5.8374	5.9552	5.9301	5.9205	5.9551
c (Å)	8.3452	8.4419	8.4155	8.4023	8.4482
V (Å^3)	284.36	299.38	295.94	294.52	299.60

TABLE II. Calculated (experimental) structural parameters of BYTO using GGA-RPBE.

	Wyckoff sites	x	y	z
Ba	4d (−4)	0	0.5	0.25
Y	2a (4/m)	0	0	0
Ta	2b (4/m)	0	0	0.5
O_1	4e (4)	0	0	0.2685 (0.2687)
O_2	8h (m)	0.2520 (0.2175)	0.2857 (0.2578)	0.0

O 2p states with d states of Ta and Y, due to the presence of Ta and Y atoms within the Ta(Y)O_6 octahedra and to lesser extent with Ba d states. The nature of chemical bonding can be elucidated from the total to partial density of states (DOS). By comparing the total DOS (Figure 2(b)) with angular momentum projected DOS (Figures 3(a)–3(d)), one can show that some electrons from p states of O, d states of Ta, and Y are transferred into valence bands (VBs) and contribute to covalent interactions between Ta(Y)-O bonds and also Ta-O bond has high covalency than Y-O bond. The conduction band is situated above E_F at around ∼3.4 eV to 6.6 eV. The conduction band around 5 eV is mainly contributed from d states of Y, Ta, and Ba as well as from O 2p states.

B. Mulliken band population

In Sec. III A, it has been shown that there exists a significant hybridization of Ta/Y 3d with O 2p states in BYTO indicating the bonding in this system cannot be purely ionic but must exhibit a covalent part. In order to have a clear picture about the nature of chemical bonding between constituent of BYTO, we have calculated Mulliken band population and Born effective charges.

The Mulliken band population is essential for evaluating the bonding character in a material. A high value of bond population indicates a covalent bond, and a low value indicates an ionic nature. Positive and negative values indicate bonding and antibonding states, respectively. The Mulliken population reported in Table III shows that the Ba-O bond exhibits almost ionic nature with slight covalency, whereas Ta/Y-O bond has mixed covalent and ionic characteristics. Since Ta-O bond has higher Mulliken population than that of Y-O bond, it is slightly more covalent than Y-O bond. Since the overlap of t_{2g} (d^0 configuration) of Ta (Figure 3(b)) is higher than that of Y (Figure 3(c)) with ligand orbitals, Ta-O bonding energy is higher than that of Y-O bonds and this lead a higher covalent character Ta-O bond than that of Y-O bond. The two different wyckoff positions of O atoms lead a small change in bond length between O_1 and O_2 with Ba, Ta, and Y ions. Further, the interatomic distance (Table III) between Ta (Y) and O is ∼1.9522 Å (∼ 2.2689 Å) and that between Ba and O is ∼2.9818 Å and 2.8870 Å (for O_1 and O_2) indicating the covalent bonding between Ta(Y) and O ions and ionic bonding between Ba and O ions. It is to be mentioned that if we consider the self-consistently calculated valence charges (Table IV), the chemical formula for the system may roughly be written as $Ba_2^{1.22}Y^{1.08}Ta^{1.51}O_6^{-0.84}$. Thus, we find a significant deviation from the charge distribution of charge balanced $Ba_2^{2}Y^{3}Ta^{5}O_6^{-2}$. The strong hybridization between O 2p states and the Ta(Y) d states reveals that the static Ta (Y) and O charges are significantly less than +5 (+3) and −2. According to the ionicity scale,[20] the population ionicity can be calculated as

$$P_i = 1 - \exp\left[-|P_c - P|/P\right], \quad (1)$$

where P is the overlap population of the bond, P_c is the bond population, for a purely covalent bond ($P_c = 0.75$). P_i is equal to zero for purely covalent bond and to unity for purely ionic bond. The Ta- O bond exhibits high covalency than Y-O bond, whereas Ba-O bond exhibits high ionicity.

C. Born effective charges

Born effective charges (Z^*) play a fundamental role in the dynamics of the crystal lattices. They govern the amplitude of the long-range coulomb interactions between nuclei and the splitting between longitudinal optic (LO) and transverse optic (TO) phonon modes. For an insulator, Z^* is a measure of change in electronic polarization due to ionic displacements. The form of effective tensor for the constituents is determined by the site symmetry of ions. Z^* is defined as the proportionality coefficient relating, at linear order, the polarization per unit cell created along the β direction, to the displacement along the direction α of the atoms belonging to the sublattice κ, under the condition of zero electric field (ε)

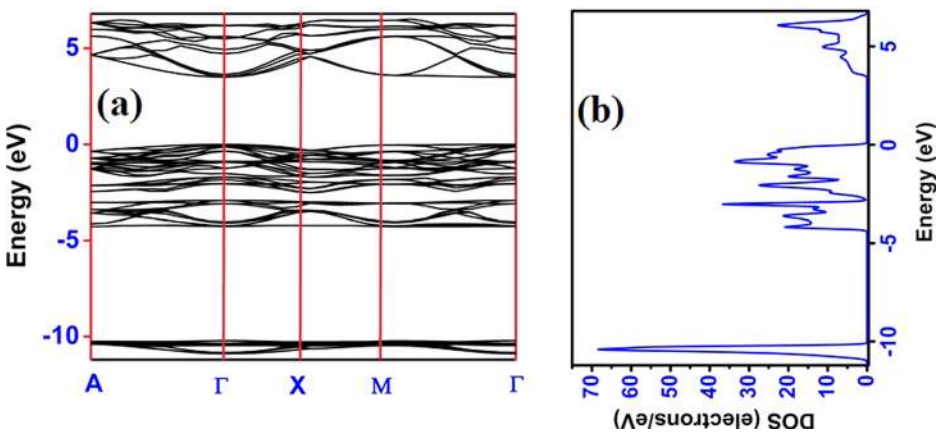

FIG. 2. (a) Electronic band structure along high symmetry directions and (b) DOS of BYTO.

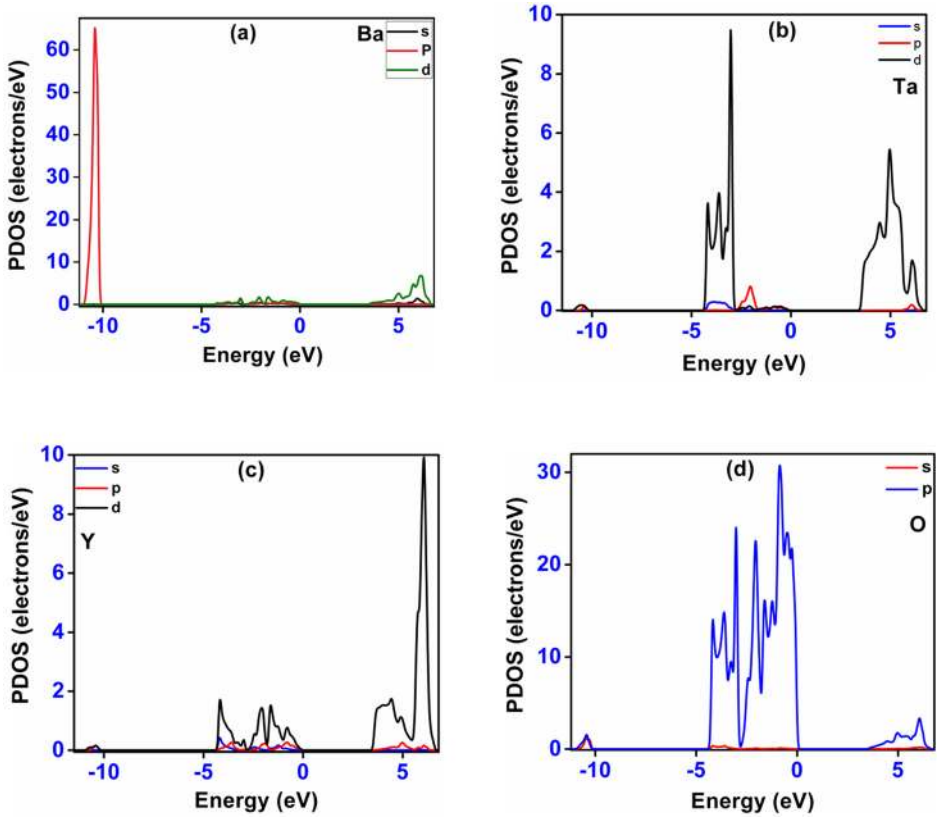

FIG. 3. Partial DOS of (a) Ba, (b) Ta, (c) Y, and (d) of BTYO. The Fermi energy is set to zero.

$$Z^*_{\alpha\beta}(\kappa) = \Omega_0 \frac{\partial P\alpha}{\partial \tau_\beta(\kappa)}\bigg|_{\varepsilon=0}, \tag{2}$$

where Ω_0 is the unit cell volume. The components of these tensors reflect the effects of covalency or ionicity with respect to some reference ionic value.

Z^* related to the atoms constituting BYTO are reported in Table IV. In this case, the cartesian x, y, and z are aligned along the crystalline [100], [010], and [001] directions. In tetragonal symmetry, the Born effective charge tensor is diagonal and reduces to values $Z^*_{xx} = Z^*_{yy} = Z^*_{\perp}$ and $Z^*_{zz} = Z^*_{\perp}$, except Z^* of O_2. The off-diagonal elements ($Z^*_{yx} = Z^*_{yx}$) arise from the tetragonal distortion due to lower site symmetry of O.[21] Since O_2 along [100] and [010] direction ((m) site symmetry, (x, y, 0)) and O_1 along [001]-direction (4 site symmetry, (0, 0, z)) is bonded with Ta (Y) atoms, a large anomalous contributions to Z^*, on Ta/Y and O_2 ions in the ab-plane and on Ta/Y and O_1 ions in the apical direction (along [001] direction). This anomalous contribution clearly indicates that a strong dynamic charge transfer takes place along the Ta/Y-O bond. When O atom is displaced closer to Ta/Y atom, the change in bond hybridization causes transfer of electrons from O to Ta (Y). This transfer of electrons results in an increase in Ta (Y) bond covalency. The deviation in large anomalous contributions of Born effective tensors, along and perpendicular to [001] direction, reflects the sensitivity to the atomic displacement of the partially covalent character of Ta/Y-O bond, owing to the point site symmetry of the ions. The charge observed on Ba indicates the ionic covalent character of bonding along 3 crystallographic directions. In the ab-plane, the value of Z^* on O_1 and along apical direction on O_2 is close to nominal value (−2) indicating the ionic character of bonding. The finite value of $Z^*_{yx} = Z^*_{yx}$ occurs due to site symmetry (m) of O_2 ions. The anisotropic diagonal elements of Z^* of O_2 and finite off-diagonal element of O_2 clearly reflect the presence of covalent bonding of interactions.[22]

TABLE III. The calculated (experimental) bond population, population ionicity, and bond length of BYTO using GGA-RPBE.

Bond	Bond population, P	Population ionicity, P_i	Bond length (Å)
Ba - O_1	0.06	0.999	2.9818 (2.979)
Ba - O_2	0.06	0.999	2.8870 (2.867)
Y - O_1	0.42	0.564	2.2687 (2.210)
Y - O_2	0.40	0.524	2.2689 (2.216)
Ta - O_1	0.57	0.271	1.9522 (2.015)
Ta - O_2	0.57	0.254	1.9516 (2.000)

In order to gain further insight into the nature of the bonding accurately, we calculate the electron density distribution for BYTO. The charge density in our calculation is derived from a reliable converged wave function and hence it can be used to study the bonding nature of solid. The total charge density plots of BYTO along [100] direction show the deviation of the spherically distributed charge density around O ions, as shown in Figure 4. Moreover, it also shows that the deviation of the spherically distributed charge density is more towards Ta atoms than Y atom, indicating the slightly high covalent nature of Ta–O bond than Y-O bond. The spherical distribution of charges around Ba ions indicates a dominated ionic nature of interaction.

TABLE IV. Components of the calculated Born effective charge tensors at the Ba, Ta, Y, and O sites of BYTO using GGA-RPBE and Mulliken charges of Ba, Ta, Y, and O.

	Z^*_{xx}	Z^*_{xy}	Z^*_{xz}	Z^*_{yx}	Z^*_{yy}	Z^*_{yz}	Z^*_{zx}	Z^*_{zy}	Z^*_{zz}	Mulliken charges |e|
Ba	2.72	0.01	0.0	−0.01	2.72	0.0	0.0	0.0	2.80	1.22
Ta	6.99	0.03	0.0	−0.03	6.99	0.0	0.0	0.0	7.00	1.51
Y	4.81	−0.12	0.0	0.12	4.81	0.0	0.0	0.0	4.84	1.08
O_1	−2.05	0.01	0.0	−0.01	−2.05	0.0	0.0	0.0	−4.55	−0.84
O_2	−3.42	−1.22	0.0	−1.25	−3.15	0.0	0.0	0.0	−2.08	−0.84

D. Vibrational properties

The linear response method was used to calculate vibrational properties of BYTO. The linear response method provides an analytical way of calculating the second derivative of the total energy with respect to perturbation. A perturbation in ionic positions yields the dynamical matrix and phonons. The lattice vibration mode with $q \approx 0$ plays a dominant role in Raman scattering and infrared absorption. Therefore, the vibration frequency at the Γ ($q = 0$) is called as normal vibration mode. Using method of factor group analysis, we determine the distribution of the zone-centre vibrational modes in terms of the representation of C_{4h} point group

$$\begin{aligned}\Gamma(I4/m) = {} & 6T(2A_u + B_g + E_g + 2E_u) \\ & + 2L(A_g + E_g) + \upsilon_1(A_g) + 2\upsilon_2(A_g + B_g) \\ & + 2\upsilon_3(A_u + E_u) + 2\upsilon_4(A_u + E_u) \\ & + 2\upsilon_5(E_g + B_g) + \upsilon_6(E_u),\end{aligned}$$

where υ_1, υ_2, and υ_3 are related to Y(Ta)-O stretching mode, and υ_4, υ_5, and υ_6 are O- Y(Ta)-O bending modes. T and L are translational and librational lattice modes, respectively. The symbols A and B represent nondegenerate and E double degenerate vibrational modes; symmetric and antisymmetric modes with respect to a centre of inversion are denoted by subscripts g and u, respectively. There are nine Raman-active and infrared (IR)-active modes that exist. In the Raman-active modes, Y and Ta atoms are at rest. Table V compares calculated frequencies at the Brillouin zone center with available experimental and theoretical results. The agreement with experimental values is typically within 5%, which is good for a first principles calculation.[23] Figure 5 shows the displacement patterns of allowed Raman modes of vibration of BYTO. Among Raman modes, three modes (95 cm^{-1}, 398 cm^{-1}, and 597 cm^{-1}) are presumably arises due to the descent to lower symmetry (cubic-tetragonal symmetry).[26] The highest Raman A_g (847 cm^{-1}) mode corresponds to the displacement of oxygen atom along Y-O-Ta axis, while all the cations are at rest. This frequency is mainly determined by the Ta-O and Y-O distances and bonding forces, and thus by the chemical nature of the Ta and Y octahedral cations. In this mode, all the O atoms are moving outward/inward, known as breathing mode.[28] In B_g (602 cm^{-1}) mode, only in-plane O_2 atoms are involved, with one diagonally opposite pair displaced outwards (inwards) and other pair displaced inwards (outwards), known as out-of-phase stretching.[29] Here, the Ba atoms are also displaced in opposite direction along c-axis. The A_g (597 cm^{-1}) mode is an octahedral stretching mode (only oxygen atoms are vibrating), where the four in-plane O_2 atoms are displaced

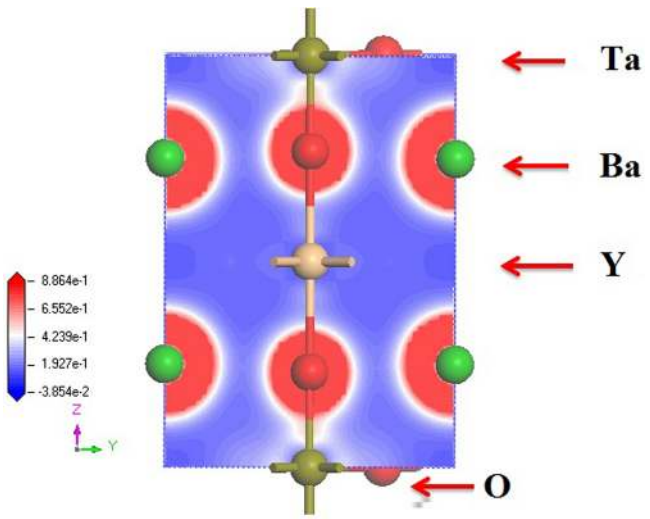

FIG. 4. Charge density distribution of BYTO along [100] direction.

TABLE V. Calculated and experimental frequencies (cm^{-1}), assignment of the Raman and IR modes of BYTO using GGA-RPBE and oscillator strength (Debye^2 Å^{-2} (amu)$^{-1}$) of IR mode. The phonon frequencies are presented in increasing order.

Symmetry	Cal.	Exp.[a,b]	Mode	Oscillator strength, $A_{\alpha\beta}$(m)	Cal.[c]	Cal.[d]
E_g^1	68		R			76.4
E_g^2	95	(105) 104	R			109.8
B_g^1	97		R			109.8
A_g^1	114	(Soft mode)	R			
E_g^3	398	(388) 384	R		390	403.7
B_g^2	403		R			403.9
A_g^2	597	(795[e]) 573	R		562	583
B_g^3	602		R		567	583.1
A_g^3	847	(838) 836	R		841	823
A_u^1	93	110	IR	24.58	125.3	
E_u^1	99		IR	17.11	124.7	
A_u^2	204		IR	112.54	210.4	
E_u^2	211		IR	88.37	211	
E_u^3	228	218	IR	26	225.3	
A_u^3	258	264	IR	0.20	270.9	
E_u^4	260		IR	5.17	271.0	
A_u^4	546	540	IR	61.41	548.5	
E_u^5	552		IR	59.53	548.3	

[a]Reference 24.
[b]Reference 25.
[c]Reference 26.
[d]Reference 27.
[e]Raman mode due to local defects.

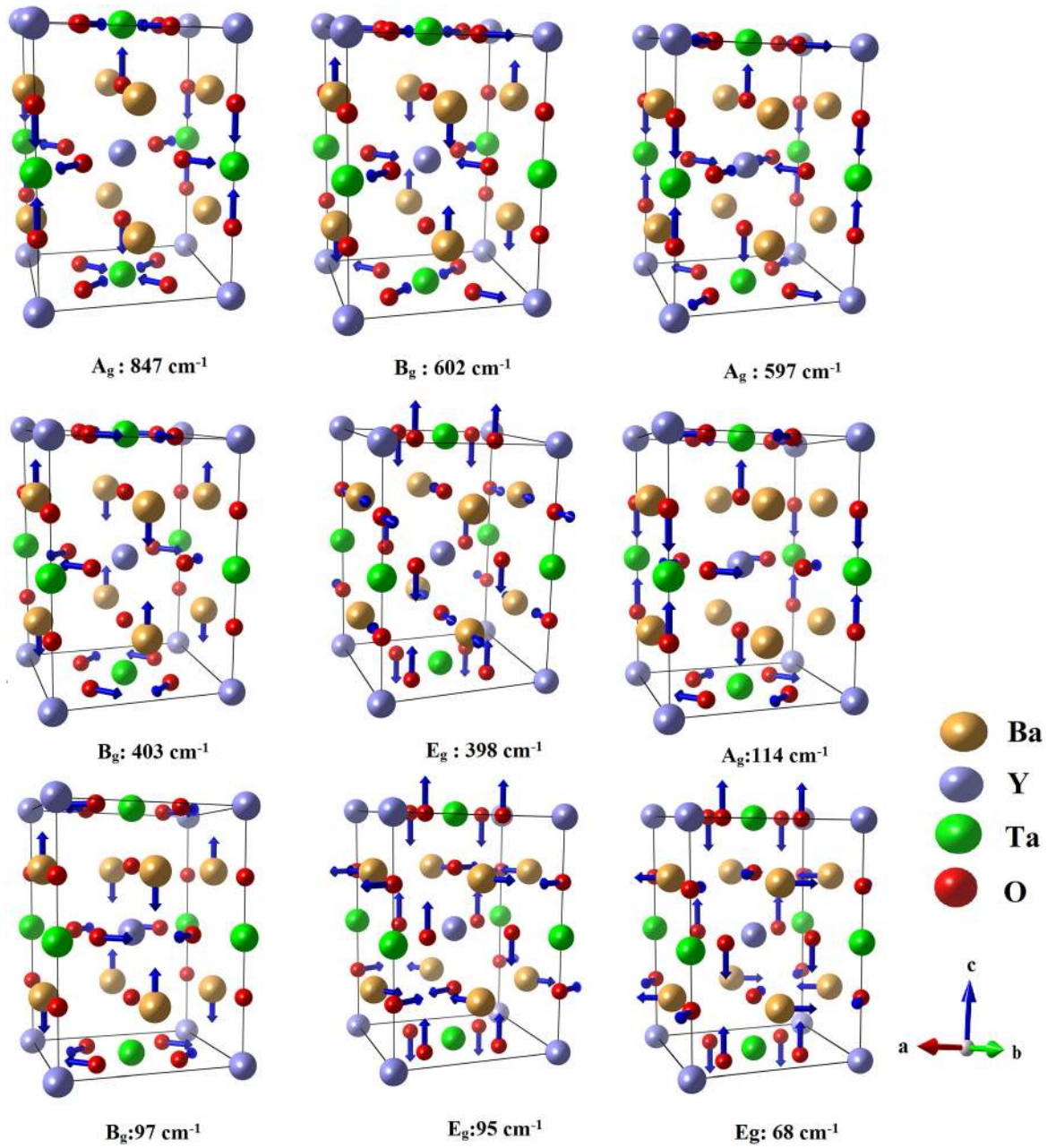

FIG. 5. Illustrations of the displacement patterns of the Raman modes of BYTO. Each displacement vector is obtained from the eigen vector by dividing each component by the square root of the corresponding atomic mass. This figure was drawn using VESTA.[17]

inwards and the two apical O atoms are displaced outwards and vice versa, known as out-of-phase stretching.[29] The B_g (403 cm^{-1}) is Raman active scissor mode, where O_2 atoms are displaced in ab-plane and Ba atoms are displaced in opposite direction along c-axis. The E_g (398 cm^{-1}) mode is an octahedral tilt mode ([110] rotation), with Ba atoms are displaced in ab-plane.[30] The A_g (114 cm^{-1}) mode is anti-phase rotations of the octahedra about [001] and O_1 atoms are displaced opposite direction along c-axis. The B_g (97 cm^{-1}) mode is a scissoring mode with Ba atoms are displaced opposite direction along c-axis. Here, O_1 atoms are not displaced.[31] In Eg (95 cm^{-1}) mode, diagonally opposite pair of O_2 atoms is displaced opposite direction along c-axis with O_1 and Ba atoms along c-axis are displaced in ab plane in opposite direction. The vibration of E_g (68 cm^{-1}) mode is similar to that of last mode (95 cm^{-1}). All E_g modes are doubly degenerate modes that involve the motion in the ab plane of the tetragonal BYTO have the same frequency and character for the displacement along either a or b axis.

Figure 6 shows the displacement patterns of allowed IR modes of vibration of BYTO. The E_u modes are an inplane mode; all atoms are displaced only in ab-plane, while in A_u modes, the atoms are displaced along c-axis. The IR modes 552 cm^{-1}, 546 cm^{-1}, 211 cm^{-1}, and 204 cm^{-1} ($2E_u$ and $2A_u$) are octahedral stretching modes.[32] The 260 cm^{-1}, 258 cm^{-1}, and 228 cm^{-1} modes ($2E_u$ and A_u) are corresponding to octahedral bending and stretching modes. The lowest frequency modes 99 cm^{-1} and 93 cm^{-1} (E_u and A_u) consist of bending vibration of octahedra along with polar motion of Ba atoms against all atoms, known as last mode.[33–35] The 204 cm^{-1}

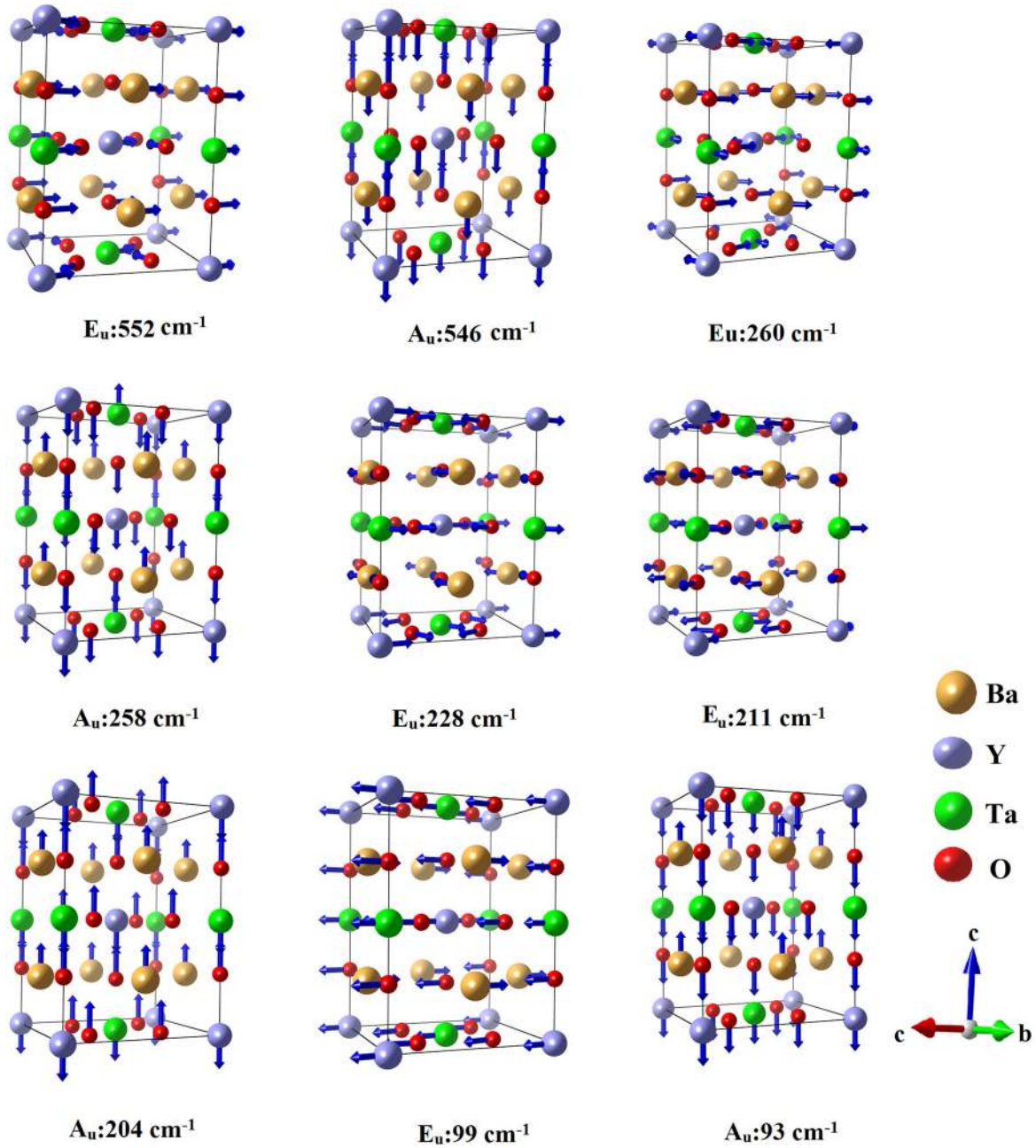

FIG. 6. Illustrations of the displacement patterns of the IR modes of BYTO. Each displacement vector is obtained from the eigen vector by dividing each component by the square root of the corresponding atomic mass. This figure was drawn using VESTA.[17]

and 211 cm^{-1} modes are known as Slater mode[33] with a contribution from Ba displacements.

E. Dielectric properties

The electronic dielectric permittivity tensor, ε^{∞}, is related to second derivative of the electronic energy with respect to electric field and has been computed using linear response method.[36] For our calculations, no scissor correction has been used. Because of the symmetry properties of tetragonal crystal structure of BYTO, this tensor is diagonal with two independent components, parallel ($\varepsilon_{zz}{}^{\infty} = \varepsilon_{||}{}^{\infty}$) and perpendicular ($\varepsilon_{xx}{}^{\infty} = \varepsilon_{yy}{}^{\infty} = \varepsilon_{\perp}{}^{\infty}$) to the tetragonal axis. The calculated values of these two independent components are $\varepsilon_{\perp}{}^{\infty} = 4.57$ and $\varepsilon_{||}{}^{\infty} = 4.61$, indicate that BYTO is a positive uniaxial ($\varepsilon_{zz}{}^{\infty}/\varepsilon_{xx}{}^{\infty} > 1$) tetragonal crystal with a quite isotropic electric response to a homogeneous field. Unfortunately, there are no available experimental or theoretical data reported in the literature for electronic dielectric permittivity tensor of BYTO for comparison purpose. Nevertheless, the magnitudes of the ε^{∞} components are similar to those observed in $BaTiO_3$ ($\varepsilon^{\infty} = 5.60$),[37] ZrO_2 ($\varepsilon^{\infty} = 4.805$), A-$La_2O_3$ ($\varepsilon^{\infty} = 4.924$),[38] $KNbO_3$ ($\varepsilon^{\infty} = 4.69$), $NaNbO_3$ ($\varepsilon^{\infty} = 4.96$), and $ZrSiO_4$ ($\varepsilon^{\infty} = 4.14$).[39]

It is well known that DFT usually overestimates the absolute values of ε^{∞} with respect to the experimental ones. This problem has been related to the lack of polarization dependence of the quasi-local (GGA) and local (LDA) exchange-correlation functionals. In spite of this error in the absolute value, the evolutions of the optical dielectric

permittivity tensor are, in general, qualitatively well described by GGA and LDA calculations.

Since electronic dielectric tensor describes the response of the electron gas to a homogeneous electric field if the ions are taken as fixed at their equilibrium positions, one need to use a model, which assimilates the solid to a system of undamped harmonic oscillator in order to include the response of the crystal lattice to the electric field. The static dielectric tensor, ε^0, can be therefore decomposed into an electronic and an ionic part such as

$$\varepsilon^0_{\alpha\beta} = \varepsilon^\infty_{\alpha\beta} + \frac{4\pi}{\Omega_0}\sum_m \frac{A_{\alpha\beta}(m)}{\omega_m^2}. \quad (3)$$

The infrared oscillator strengths, A, are a second–order tensor given by

$$A_{\alpha\beta}(m) = \left[\sum_{\gamma,\kappa}\frac{Z^*_{\alpha\gamma}(\kappa)}{\sqrt{M_\kappa}}e_\gamma(\kappa,m)\right]^*\left[\sum_{\gamma,\kappa}\frac{Z^*_{\beta\gamma}(\kappa)}{\sqrt{M_\kappa}}e_\gamma(\kappa,m)\right], \quad (4)$$

where the sums run over all atoms κ and space directions Υ, M_k is the mass of the κth atom, and $e_\Upsilon(\kappa,m)$ and ω_m are, respectively, $\Upsilon\kappa$ component of the eigen vector and the frequency of the mth mode obtained from the diagonalization of the analytical part of the dynamical matrix. The relevant components of the oscillator strength tensor (parallel-parallel component for A_{2u} modes and the perpendicular-perpendicular component for E_u modes) are given in Table V. According to the symmetry of BYTO structure, ε^0 is a diagonal tensor with two different components $\varepsilon^0{}_\perp = 36.58$ and $\varepsilon^0{}_{||} = 45.51$. From Table V, it is found that the IR modes $A_u{}^1$ ($93\,cm^{-1}$) and $A_u{}^2$ ($204\,cm^{-1}$) have small (large) oscillator strength (frequency) and they almost equally contribute to $\varepsilon^0{}_{||}$. In addition to that, $E_u{}^1$ ($99\,cm^{-1}$) and $E_u{}^2$ ($211\,cm^{-1}$) have also nearly equally contribute to $\varepsilon^0{}_\perp$, smaller than that of $A_u{}^1$ and $A_u{}^2$ and explains why $\varepsilon^0{}_{||}$ is slightly higher than $\varepsilon^0{}_\perp$. By contrast to ε^∞, the inclusion of ionic contribution results in an anisotropic ε^0 with $\varepsilon^0{}_{||}$ slightly higher than $\varepsilon^0{}_\perp$. The dielectric response of BYTO is therefore mainly ionic with slightly higher value of ε^0 along optical axis (c-axis) than in orthogonal plane (ab plane). In order to compare our results with experimental data, we average the values of ε^0 parallel and perpendicular to c-axis. The average value of ε^0 obtained by taking one third of the trace of respective dielectric tensors ($[2\varepsilon^0{}_{||} + \varepsilon^0{}_\perp]/3$) is 39.55, close to experimentally observed value 32.5 around $T_c \sim 253\,K$.[8] The calculated dielectric tensor component values are expected to be overestimated due to underestimation of band gaps in DFT calculation and it is attributed to the lack of polarization dependence in the exchange-correlation functional.

F. Elastic properties

Elastic constants characterize the ability of a material to deform under small stresses. The elastic tensor c_{ij} is determined by performing six finite distortions of the lattice and deriving the elastic constants from strain-stress relationship.[38] Because of the symmetry of the *I4/m* structure of BYTO, these tensors have only 6 independent elements to be determined. The mechanical stability in a tetragonal crystal is determined by Born's mechanical stability condition, the requirement that the crystal be stable against any homogenous elastic deformation, as follows:

$$\left.\begin{aligned}(C_{11}-C_{12})>0,\ (C_{11}+C_{33}-2C_{13})>0\\ C_{11}>0,\ C_{33}>0,\ C_{44}>0,\ C_{66}>0,\\ (2C_{11}+C_{33}+2C_{12}+4C_{13})>0\end{aligned}\right\}. \quad (5)$$

The elastic constants of our calculation in Table VI satisfy all the stability conditions. In particular, C_{12} is smaller than C_{11}, and C_{13} is smaller than the average of C_{11} and C_{33}. The other elastic properties (bulk modulus (B) and shear modulus (G)) can be calculated based on the calculated elastic constants c_{ij}. In the calculation of elastic moduli, there are two different theories, Reuss theory and Voigt theory.[41] The bulk B_R (B_V) and shear G_R (G_V) modulus using Reuss theory (Voigt theory) are given as follows:

$$B_V = \frac{1}{9}\left((c_{11}+c_{22}+c_{33})+2(c_{12}+c_{23}+c_{31})\right), \quad (6)$$

$$G_V = \frac{1}{15}\left((c_{11}+c_{22}+c_{33})-(c_{12}+c_{23}+c_{31})+3(c_{44}+c_{55}+c_{66})\right), \quad (7)$$

$$\frac{1}{B_R} = (s_{11}+s_{22}+s_{33})+2(s_{12}+s_{23}+s_{31}), \quad (8)$$

$$\frac{15}{G_R} = 4(s_{11}+s_{22}+s_{33})-4(s_{12}+s_{23}+s_{31})+3(s_{44}+s_{55}+s_{66}), \quad (9)$$

where c_{ij} and s_{ij} are the elastic stiffness coefficients and the elastic compliance coefficients, respectively. For tetragonal system, c_{22} equals c_{11}, c_{23} equals c_{13}, and c_{55} equals c_{44}. s_{ij} is the inverse matrix of c_{ij} and vice versa. It is known that the Voigt bound is obtained by the average polycrystalline moduli based on the assumption of uniform strain throughout a polycrystal and is the upper limit of the actual effective moduli,[42] while the Reuss bound is obtained by assuming a uniform stress and is the lower limit of the actual effective moduli.[43] The arithmetic average of Voigt and Reuss bounds is termed as the Voigt-Reuss-Hill approximations.[41] Bulk B_H and shear G_H moduli using Hill theory are given as follows:

$$B_H = (B_V + B_R)/2, \quad (10)$$

$$G_H = (G_V + G_R)/2. \quad (11)$$

TABLE VI. Calculated properties of BYTO using GGA-RPBE including elastic constants c_{ij}'s (GPa), bulk modulus B (GPa), and shear modulus G (GPa) in Voigt-Reuss-Hill approaches, B/G ration, Young's modulus E (GPa), and Poisson ratio υ in Hill approach.

C_{11}	C_{12}	C_{13}	C_{33}	C_{44}	C_{66}	G_V	G_R	G_H	B_V	B_R	B_H	B_H/G_H	E	υ
315.25	185.21	54.57	333	64.2	129.72	96.23	82.40	89.32	172.47	169.48	170.97	1.91	221.86	0.26

If B_H/G_H (Pugh criterion) is lesser (bigger) than 1.75, the material is considered brittle (ductile).[44] By combining mechanical stability restrictions with Eq. (8), one can easily obtain $\frac{1}{3}(C_{12}+2C_{13}) < B_V < \frac{1}{3}(C_{11}+2C_{33})$. It implies that bulk modulus B_V (172.47 GPa) must be larger than the weighted average of C_{12} and C_{13} (119.9 GPa), and smaller than the weighted average of C_{11} and C_{33} (302.03) and also the condition $\frac{1}{3}(C_{12}+2C_{13}) < B_H < \frac{1}{3}(C_{11}+2C_{33})$ is satisfied. Since BYTO possesses tetragonal symmetry with c-axis as a high symmetry axis, the elastic stiffness constants C_{11}, C_{22}, C_{33} can be directly related to the crystallographic a, b, and c-axis, and C_{44}, C_{55}, and C_{66} indicates the shear elasticity applied to the two-dimensional rectangular lattice in the (100), (010), and (001) planes. The weakest elastic stiffness constant C_{11} and C_{22} than C_{33} represents weakness of lattice interaction along crystallographic a and b-axis. Moreover, the C_{44} and C_{55} found to have weakest shear stiffness constant, indicating the soft shearing transformation along (100) and (010), respectively. The observed weakest stiffness constants and shear stiffness constant are mainly due to the out of phase $Ta(Y)O_6$ octahedra tilting about c-axis.

The analysis of elastic anisotropy is of great significance for understanding the mechanical properties of crystal. Young's modulus and Poisson ratio are important parameters for selecting materials in engineering design. Young's modulus E and Poisson's ratio υ are obtained by the following formulas:[40]

$$E = 9BG/(3B+G), \tag{12}$$

$$\upsilon = (3B-2G)/(2(3B+G)). \tag{13}$$

From the predicted value B_H and G_H in Table VI, the Young's modulus and poisson's ratio of BYTO are 221.86 GPa and 0.26, respectively. The calculated poisson ratio (0.26) is similar to that of other pinning materials $BaZrO_3$ (0.237),[45] Y_2O_3 (0.257),[46] and $BaCeO_3$ (0.294).[47] Also, the calculated Young's modulus (221.86 GPa) is similar to that of $BaZrO_3$ (229 ± 4 GPa)[48] and Y_2O_3 (198.562 GPa),[46] but higher than that of $BaCeO_3$ (109.6 GPa).[47]

In the present work, we use universal elastic anisotropy index A^U ($A^U = 5G_V/G_R + B_V/B_R - 6$) for crystal with any symmetry to estimate the anisotropic characteristic of tetragonal BYTO. For isotropic materials, $A^U = 0$. If the value of A^U deviates from zero, the material has larger anisotropy. For tetragonal BYTO, the predicted value is 0.856 slightly deviates from 0, indicating the small elastic anisotropy characteristics of BYTO. In addition, the anisotropy indexes of bulk and shear moduli (A_B and A_G) proposed by Chung and Buessen[49] are used to estimate the anisotropic characteristics of the system are given as

$$A_B = (B_V - B_R)/(B_V + B_R), \tag{14}$$

$$A_G = (G_V - G_R)/(G_V + G_R), \tag{15}$$

where $A_B = A_G = 0$ represents elastic isotropic and $A_B = A_G = 1$ represents the maximum anisotropy. For tetragonal BYTO, A_B and A_G are 0.0087 and 0.0774, which are far away from 1, suggesting again existence of a small compression and shear anisotropy. This is the first prediction of elastic properties of tetragonal BYTO and yet to be verified experimentally.

Further, we also estimated the Debye temperature Θ_D, which is an important fundamental quantity that related to many physical properties such as specific heat.[50] At low temperatures, vibrational excitations arise from acoustic vibrations and Θ_D from elastic constants is the same as that from specific heat measurements. Debye temperature can be estimated from the average sound velocity υ_m:[51]

$$\Theta_D = \frac{h}{k}\left(\frac{3n}{4\pi}\frac{N_A\rho}{M}\right)^{\frac{1}{3}}\upsilon_m, \tag{16}$$

where h is plank constant, k is Boltzmann's constant, N_A is Avogadro's number, ρ is the density, M is the molecular weight, and n is the number of atoms in the unit cell. The average sound velocity υ_m is approximately calculated from

$$\upsilon_m = \left[\frac{1}{3}\left(\frac{2}{\upsilon_l^3}+\frac{1}{\upsilon_t^3}\right)\right]^{-\frac{1}{3}}, \tag{17}$$

where υ_l and υ_t are longitudinal and transverse sound velocities, respectively, can be obtained from Navier's equation[50] as follows:

$$\upsilon_l = \sqrt{(3B+4G)/3\rho}, \tag{18}$$

$$\upsilon_t = \sqrt{G/\rho}. \tag{19}$$

The calculated values of υ_l, υ_t, and υ_m are 5.64 km/s, 3.54 km/s, and 4.46 km/s, which yield a Θ_D of 537.7 K, close to those obtained for Ba_2MgWO_6 (570 K),[52] $SrRuO_3$ (525.5 K),[53] $BaSnO_3$ (522 K),[54] and other pinning material in HTS BaZrO3 (544 K)[55] and Y_2O_3 (533.42 K).[48]

IV. CONCLUSIONS

In summary, the band structure, bonding analysis, vibrational, dielectric, and elastic properties of Ba_2YTaO_6 were investigated using first principles calculations are based on density functional theory. The calculated electronic band structure results indicated that the compound is an insulator with a direct band gap of 3.50 eV. An inspection of Mulliken population, born effective charges, and distribution of charge density shows that this material has mixed ionic–covalent character. The Raman and infrared active phonon modes are calculated and properly assigned. The calculated and measured phonon energies are in good agreement. The electronic dielectric tensor of Ba_2TaYO_6 is nearly isotropic, and the magnitude of its components is similar to those reported in ferroelectric materials. The static dielectric permittivity constants have been computed and found that the average static dielectric constant is in good agreement with experiment. A detailed analysis of the contribution of the different vibrational modes to the static dielectric constant has been performed, including the computation of oscillator strength. By contrast to electronic dielectric tensor, its static dielectric tensor is anisotropic in plane orthogonal to the optical axis of this material. The calculation of elastic constants has been

performed and satisfies the Born mechanical stability criteria for tetragonal materials, indicates the fact that the Ba_2YTaO_6 is mechanically stable. Other elastic properties, including bulk modulus, shear modulus, Young's modulus, Poisson's ratio, and elastic anisotropy ratios are also investigated. The calculated Poisson's ratio is similar to that of other pinning materials.

ACKNOWLEDGMENTS

We gratefully acknowledge to Department of Biotechnology, India for the financial support to procure CASTEP. We also thank to Dr. A. Gopalakrishna, Department of Biotechnology- IIT Madras for his help to procure and use CASTEP. The authors thankfully acknowledge the computer resources, technical expertise, and assistance provided by the High Performance Computing Environment (HPCE), IIT Madras. The crystal structure and vibrational modes are drawn using VESTA software.

[1]P. Lunkenheimer, S. Krohns, S. Riegg, S. G. Ebbinghaus, A. Reller, and A. Loidl, Eur. Phys. J. Spec. Top. **180**, 61 (2009).
[2]B. Raveau, A. Maignan, C. Martin, and M. Hervieu, Chem. Mater. **10**, 2641 (1998).
[3]C. N. R. Rao, Ferroelectrics **102**, 297 (1990).
[4]M.-H. Phan and S.-C. Yu, J. Magn. Magn. Mater. **308**, 325 (2007).
[5]M. Fiebig, J. Phys. D: Appl. Phys. **38**, R123 (2005).
[6]M. W. Lufaso and P. M. Woodward, Acta Crystallogr., Sect. B: Struct. Sci. **57**, 725 (2001).
[7]P. M. Woodward, Acta Crystallogr., Sect. B: Struct. Sci. **53**, 32 (1997).
[8]R. Zurmuhlen, E. L. Colla, D. C. Dube, J. Petzelt, I. Reaney, A. Bell, and N. Setter, J. Appl. Phys. **76**, 5864 (1994).
[9]M. W. Lufaso, R. B. Macquart, Y. Lee, T. Vogt, and H.-C. Loye, Chem. Commun. 168 (2006).
[10]A. Llordés, A. Palau, J. Gázquez, M. Coll, R. Vald, A. Pomar, J. Arbiol, R. Guzmán, S. Ye, V. Rouco, F. Sandiumenge, S. Ricart, T. Puig, M. Varela, D. Chateigner, J. Vanacken, J. Gutiérrez, V. Moshchalkov, G. Deutscher, C. Magen, and X. Obradors, Nature Mater. **11**, 329 (2012).
[11]M. D. Segall, P. J. D. Lindan, M. J. Probert, C. J. Pickard, P. J. Hasnip, S. J. Clark, and M. C. Payne, J. Phys.: Condens. Matter **14**, 2717 (2002).
[12]T. H. Fischer and J. Almlof, J. Phys. Chem. **96**, 9768 (1992).
[13]A. Kjekshus, T. Rakke, and A. F. Anderson, Acta Chem. Scand. Ser. A **28**, 996 (1974).
[14]T. A. Bitter, C. T. Prewitt, J. L. Gillson, P. E. Bierstedt, R. B. Flippen, and H. S. Young, Solid State Commun. **4**, 533 (1966).
[15]S. Baroni, S. de Gironcoli, A. Dal Corso, and P. Giannozzi, Rev. Mod. Phys. **73**, 515 (2001).
[16]A. M. Glazer, Acta Crystallogr., B **28**, 3384 (1972).
[17]K. Momma and F. Izumi, J. Appl. Crystallogr. **44**, 1272 (2011).
[18]G. Q. Lin, H. Gong, and P. Wu, Phys. Rev. B **71**, 085203 (2005).
[19]S.-P. Huang, W.-D. Cheng, D.-S. Wu, J.-M. Hu, J. Shen, Z. Xie, H. Zhang, and Y.-J. Gong, Appl. Phys. Lett. **90**, 031904 (2007).
[20]J. He, E. Wu, H. Wang, R. Liu, and Y. Tian, Phys. Rev. Lett. **94**, 015504 (2005).
[21]J. Ławewski, P. T. Jochym, and K. Parlinski, J. Chem. Phys. **117**, 2726 (2002).
[22]N. Li, K. Yao, G. Gao, Z. Sun, and L. Li, Phys. Chem. Chem. Phys. **13**, 9418 (2011).
[23]W. Zhong, R. D. King-Smith, and D. Vanderbilt, Phys. Rev. Lett. **72**, 3618 (1994).
[24]I. Gregora, J. Petzelt, J. Petzelt, J. Pokorný, V. Vorlíček, and Z. Zikmund, Solid State Commun. **94**, 899 (1995).
[25]Q. Zhou, B. J. Kennedy, and J. A. Kimpton, J. Solid State Chem. **184**, 729 (2011).
[26]W. Li, L. Ning, and P. A. Tanner, J. Phys. Chem. A **116**, 7337 (2012).
[27]H. C. Karandeep, S. Gupta, and S. Kumar, J. Alloys Compd. **555**, 335 (2013).
[28]K. Kunc, R. Zeyher, A. I. Liechtenstein, M. Methfessel, and O. K. Andersen, Solid State Commun. **80**, 325 (1991).
[29]M. N. Iliev, M. V. Abrashev, H.-G. Lee, V. N. Popov, Y. Y. Sun, C. Thomsen, R. L. Meng, and C. W. Chu, Phys. Rev. B **57**, 2872 (1998).
[30]W. Wei-Ran, X. Da-Peng, and S. Wen-Hui, Chin. Phys. Lett. **22**, 705 (2005).
[31]M. C. Weber, J. Kreisel, P. A. Thomas, M. Newton, K. Sardar, and R. I. Walton, Phys. Rev. B **85**, 054303 (2012).
[32]J. T. Last, Phys. Rev. **105**, 1740 (1957).
[33]K. Z. Rushchanskii, N. A. Spaldin, and M. Ležaić, Phys. Rev. B **85**, 104109 (2012).
[34]J. D. Axe, Phys. Rev. **157**, 429 (1967).
[35]J. Harada, J. D. Axe, and G. Shirane, Acta Crystallogr., A **26**, 608 (1970).
[36]X. Gonze and C. Lee, Phys. Rev. B **55**, 10355 (1997).
[37]P. Ghosez, X. Gonze, and J. P. Michenaud, Ferroelectrics **153**, 91 (1994).
[38]R. Vali and S. M. Hosseini, Comput. Mater. Sci. **31**, 125 (2004).
[39]R. Puthenkovilakam, E. A. Carter, and J. P. Chang, Phys. Rev. B **69**, 155329 (2004).
[40]S. L. Shang, T. Wang, and W. Z. K. Liu, Appl. Phys. Lett. **90**, 101909 (2007).
[41]R. Hill, Proc. Phys. Soc. London, Sect. A **65**, 349 (1952).
[42]W. Voigt, *Lehrburch der Kristallphysik* (Teubner, Leipzig, 1928).
[43]A. Reuss, Z. Angew. Math. Mech. **9**, 49 (1929).
[44]S. F. Pugh, Philos. Mag. **45**, 823 (1954).
[45]K. C. Goretta, E. T. Park, R. E. Koritala, M. M. Cuber, E. A. Pascual, N. Chen, A. R. de Arellano López, and J. L. Routbor, Physica C **309**, 245 (1998).
[46]H. A. Badehian, H. Selehi, and M. Ghoohestani, J. Am. Ceram. Soc. **96**, 1832 (2013).
[47]Z. Zhang, J. Koppensteiner, W. Schranz, J. B. Betts, A. Migliori, and M. A. Carpenter, Phys. Rev. B **82**, 014113 (2010).
[48]D. Dierickx, I. Houben, J. Lapin, F. Delannay, and O. Van der bist, J. Mater. Sci. Lett. **15**, 1573 (1996).
[49]D. H. Chung and W. R. Buessem, *Anisotropy in Single Crystal Refractory Compounds* (Plenum, New York, 1968), Vol. 2.
[50]R. Ravindran, L. Fast, P. A. Korzhavyi, B. Johansson, J. Wills, and O. Eriksson, J. Appl. Phys. **84**, 4891 (1998).
[51]O. L. Anderson, J. Phys. Chem. Solids **24**, 909 (1963).
[52]L. Shi, L. Wu, Y. F. Duan, J. Hu, X. Q. Yang, G. Tang, and L. Z. Hao, Eur. Phys. J. B **86**, 9 (2013).
[53]T. Kiyama, K. Yoshimura, K. Kosuge, Y. Ikeda, and Y. Bando, Phys. Rev. B **54**, R756(R) (1996).
[54]T. Maekawa, K. Kurosaki, and S. Yamanaka, J. Alloys Compd. **416**, 214 (2006).
[55]S. Yamanaka, M. Fujikane, T. Hamaguchi, H. Muta, T. Oyama, T. Matsuda, S.-i. Kobayashi, and K. Kurosaki, J. Alloys Compd. **359**, 109 (2003).